Dynamic characterization of 3D printed lightweight structures

Advances in Aircraft and Spacecraft Science, *Vol. 9, No. 4 (2022) 301-318*
https://doi.org/10.12989/aas.2022.9.4.301

Dynamic characterization of 3D printed lightweight structures

Mohamed Refat*[1,2], Enrico Zappino[2a], Alberto Racionero Sánchez-Majano[2b] and Alfonso Pagani[2c]

[1]*Department of Industrial Engineering, University of Bologna, Vialedel Risorgimento,2,40136 Bologna, Italy*
[2]*MUL2 Group, Department of Mechanical and Aerospace Engineering, Politecnico di Torino, Corso Duca degli Abruzzi 24, 10129 Torino, Italy*

(Received June 12, 2022, Revised July 29, 2022, Accepted August 30, 2022)

Abstract. This paper presents the free vibration analysis of 3D printed sandwich beams by using high-order theories based on the Carrera Unified Formulation (CUF). In particular, the component-wise (CW) approach is adopted to achieve a high fidelity model of the printed part. The present model has been used to build an accurate database for collecting first natural frequency of the beams, then predicting Young's modulus based on an inverse problem formulation. The database is built from a set of randomly generated material properties of various values of modulus of elasticity. The inverse problem then allows finding the elastic modulus of the input parameters starting from the information on the required set of the output achieved experimentally. The natural frequencies evaluated during the experimental test acquired using a Digital Image Correlation method have been compared with the results obtained by the means of CUF-CW model. The results obtained from the free-vibration analysis of the FDM beams, performed by higher-order one-dimensional models contained in CUF, are compared with ABAQUS results both first five natural frequency and degree of freedoms. The results have shown that the proposed 1D approach can provide 3D accuracy, in terms of free vibration analysis of FDM printed sandwich beams with a significant reduction in the computational costs.

Keywords: additive manufacturing; Carrera unified formulation; digital image correlation; fused deposition modeling; inverse problem; material characterization

1. Introduction

Three-dimensional (3D) printing, also referred to as Additive Manufacturing (AM), presents a new paradigm on how products are designed and fabricated (Goh *et al*. 2021). Fused Deposition Modeling (FDM) technology is an AM method that is extensively used for creating intricate geometrical parts (Penumakala *et al*. 2020). Among various AM techniques, FDM is a promising technique that is gaining a wide recognition for producing complex continuous fiber composites parts regardless of manufacturing skills or labour cost (Gibson *et al*. 2021, Refat *et al*. 2021)

*Corresponding author, Ph.D. Student, E-mail: mohamedrefat.ramada2@unibo.it
[a]Assistant Professor, E-mail: enrico.zappino@polito.it
[b]Ph.D. Student, E-mail: alberto.racionero@polito.it
[c]Associate Professor, E-mail: alfonso.pagani@polito.it

http://www.techno-press.org/?journal=aas&subpage=7 ISSN: 2287-528X (Print), 2287-5271 (Online)

owing to its inexpensive machines, easy to use, low material wastage (Caminero *et al*. 2018, Chacón *et al*. 2017), and variety of materials to be used including plastics, ceramics, composites and metal powder (Penumakala *et al*. 2020, Turner and Gold 2015, Turner *et al*. 2014). For instance, FDM is utilised to create complex lightweight structures in aerospace applications Kumar and Krishnadas Nair (2017), automotive industries (Lee *et al*. 2017), printing organs and tissues in medical fields Zadpoor and Malda (2017), and structural models in architecture applications (Caminero *et al*. 2018, Chacón *et al*. 2017, Gao *et al*. 2015, Hofstätter *et al*. 2017, Melenka *et al*. 2016, Parandoush and Lin 2017, Wang *et al*. 2017). FDM creates a part via laying-up material according to the layer-by-layer approach (Cuellar *et al*. 2018, Gibson *et al*. 2021), in which filament material is extruded from a heated nozzle, which then deposits the first layer to start creating the part in the semi solid state (Penumakala *et al*. 2020). FDM machines usually consist of a printing bed, build platform, build material spool and liquefier head. Although most of 3D printed parts are only used as a prototypes rather than end use applications, FDM have brought about a paradigm shift on manufacturing finished functional parts (Caminero *et al*. 2018). FDM of composites can remove limitations of producing primary structural parts by embedding reinforcement into the matrix and, by doing so, a more functional part can be produced (Caminero *et al*. 2018, Van Der Klift *et al*. 2016, Wang *et al*. 2017). Several types of reinforcement including short fibers, continuous carbon fibers, and Onyx have been used (Berretta *et al*. 2017, Caminero *et al*. 2018, Ferreira *et al*. 2017, Ivey *et al*. 2017, Ning *et al*. 2015, Parandoush and Lin 2017, Tekinalp *et al*. 2014). Onyx is a chopped fiber embedded in a rigid nylon and can be utilised alone or integrated with Kevlar, glass or continuous carbon fibers (Bárnik *et al*. 2019). Onyx becomes the ideal material to produce functional parts that met industry requirements (Bárnik *et al*. 2019). The addition of fibers provides stiffness and heat resistance up to 145°C integrated with the toughness of nylon (Bárnik *et al*. 2019). For example, Markforged® company claimed that, parts printed with Onyx are 30% stiffer and stronger opposed to similar products produced by other 3D printers (Bárnik *et al*. 2019), Markforged.

FDM printed parts exhibit complex behavior since the components are composed by several entities, i.e., infill, floor, roof and wall components in each layer having different material and geometrical properties. Most studies rely on the experimental work to characterize material properties and since setting up experimental work are laborious as an extensive experimental tools is required, a paradigm to obtain the properties via a numerical tool is a challenge. For example, a lot of research was carried out to investigate property structure relationship in 3D printing/FDM to understand the effects of several parameters such as printing temperature, infill angle, densities and layer thickness (Afrose *et al*. 2016, Akhoundi and Behravesh 2019, Ding *et al*. 2019, Durgun and Ertan 2014, Gibson *et al*. 2021, Gordelier *et al*. 2019, Rajpurohit and Dave 2018, Sanei and Popescu 2020, Vălean *et al*. 2020). (Gordelier *et al*. 2019) optimized the FDM process to achieve maximum tensile strength and demonstrated that by tuning printing design process, mechanical properties could be raised by 50%. (Afrose *et al*. 2016) studied the influence of part build orientations on fatigue behavior of FDM. It was shown an increase of 20% in strength for unreinforced PLA via printing the infill at 0° with respect to the loading direction instead of 90°. (Melenka *et al*. 2016) obtained elastic properties of Kevlar reinforced structures printed by a MarkOne and used an analytical method based on volume average stiffness method (VAS) to predict the elastic properties. (Al Abadi *et al*. 2018) developed mathematical expressions for assessing elastic properties of fiber reinforced structures printed using FDM. Further, most of the FDM printed parts have hygroscopic properties and hence it is vital to account moisture absorption behavior and so it affects the mechanical performance (Lay and Thajudin 2019, Ma *et al*. 2021,

Miri *et al*. 2009, Valentin *et al*. 1987). Therefore, rigorous models are needed to provide a clear understanding of their structural performance without the need for many experimental work. Several numerical studies have been carried out for the analysis of the FDM parts. For example, Masrol and Siswanto (2014) carried out a numerical simulation using various element types. (Coelho *et al*. 2015) used the available predictive capabilities in commercial finite element analysis software ABAQUS. (Al Abadi *et al*. 2018) uses the latter software to predict the damage and failure modes in the FDM printed coupons. Given the mentioned previous work, and in addition to, existing micro and meso numerical models are exhibited in the literature to simulate and analyze the mechanical behavior of FDM printed part (Li *et al*. 2002). However, there is still a gap in obtaining the material properties used (e.g., elastic modulus) as it is usually unknown and sensitive to such specific parameters used (e.g., infill density), making the numerical simulation elusive and inaccurate.

To circumvent that research absence, developing a numerical solution for the analysis of such printed structures is of a particular interest. In view of this, Carrera Unified Formulation (CUF) has been applied to provide accurate analysis of printed specimens with lower computational cost. CUF describes the kinematic field in an unified approach that will be then used to derive the governing equation in a hierarchical compact manner (Azzara *et al*. 2020, Carrera and Petrolo 2012, Carrera *et al*. 2011, 2017). The current work aims to model the FDM printed parts in a reliable and accurate method within a low computational cost and then to characterize the material properties based on the inverse problem formulation. The inverse problem approach proceeds in the opposite direction with respect to standard forward models. Leverage the resulting numerical model to build a data driven model that allows obtaining directly the material properties used without the need of extensive experimental works. Free vibration experimental test has been performed to validate the accuracy of the above mentioned approach. Specimens have been printed by using the 3D printer MarkTwo® (MT) provided by Markforged® company. The first fundamental frequency and mode was evaluated by using the Digital Image Correlation (DIC) technique (Chu *et al*. 1985, Dai *et al*. 2017, Zappino *et al*. 2020).

The paper is organized as follows: First, Lagrange (LE) and Taylor (TE) expansions CUF models, including the governing differential equations of free vibration analysis, are presented in Section 2.

Second, experimental setup of selected beams are used to validate the proposed numerical model as shown in Section 3. Third, numerical analysis and results are presented in Section 4. Such analysis and results comprise the implementation of proposed method to model FDM parts and the material characterization based on inverse problem are presented. Finally, some meaningful conclusions based on the above analysis are obtained.

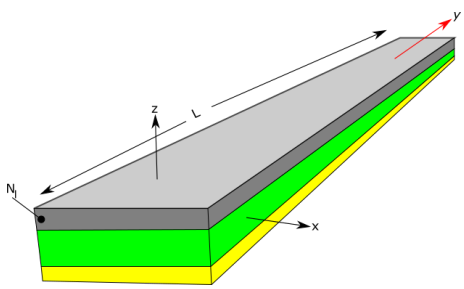

Fig. 1 3D printed Laminated beam and its related Cartesian coordinate system

2. Carrera unified formulation

Let us consider a generic 3D printed laminated beam structure with N_l layers and length L as depicted in Fig. 1. A Cartesian coordinate frame is used, in which x and z are the cross-section coordinates and y is orthogonal and places along the beam axis (in red). According to the CUF framework, 3D displacement field $\boldsymbol{u}$ of the FDM parts can be expressed as the product of two elements: one along the beam axis and one over the cross-section (Petrolo *et al*. 2016). For example, in a 1D model, the beam contribution is referred to the beam axis y. Instead the other contribution is a function of x and z and hence the 3D displacement field becomes as the following

$$\boldsymbol{u}(x,y,z) = F_\tau(x,z)\boldsymbol{u}_\tau(y), \qquad \tau = 1,2,\dots,M \tag{1}$$

in which, F_τ represents the function expansion depending on the beam cross-section coordinates x and z. $\boldsymbol{u}_\tau$ is the generalized displacement vector, and M refers to the number of the expansion terms. Based on Einstein notation, subscript τ stands for summation on the number of terms in the expansion. The choice of both terms F_τ and M is arbitrary, that is, various base functions of any order can be chosen to model the kinematic field of a beam (Azzara *et al*. 2020, Carrera *et al*. 2014, Pagani *et al*. 2014, 2022, Shen *et al*. 2022). The Finite Element Method (FEM) is applied to discretize the beam along y-axis. Hence, the generalized displacements $\boldsymbol{u}_\tau$ are defined as functions of the unknown nodal displacement vector $\boldsymbol{q}_{\tau i}$ and the 1D shape functions $\boldsymbol{N}_i$ is illustrated below

$$\boldsymbol{u}_\tau(y) = \boldsymbol{N}_i\,\boldsymbol{q}_{\tau i}, \qquad i = 1,2,\dots,k \tag{2}$$

In this work, both Lagrange and Taylor polynomials are used for F_τ functions. In which, cross section is divided into local expansion sub-domains, to be able to account complex beam shapes.
Lagrange polynomials are used with respect to normalized coordinates and can be many types such as quadrilateral Lagrange polynomials, four-point (L4) bilinear, nine-point (L9) bi-quadratic, and 16-point (L16) bi-cubic. In this work, only L9 is used. Its interpolation functions are given by

$$\begin{aligned} F_\tau &= \frac{1}{4}\,(r^2 + rr_\tau)(s^2 + ss_\tau), \qquad \tau = 1,3,5,7 \\ F_\tau &= \frac{1}{2}s_\tau^2\,(s^2 + ss_\tau)(1-r) + \frac{1}{2}r_\tau^2(r^2 + rr_\tau)(1-s^2) \qquad \tau = 2,4,6,8 \\ F_\tau &= (1-r^2)(1-s^2), \qquad \tau = 9 \end{aligned} \tag{3}$$

where r and s range from -1 and +1. Therefore, based on different elements, the cross-section displacement fields can be represented after substituting in Eq. (1). For instance, the complete displacement field of one single L9 element is as follows

$$\begin{aligned} u_x &= F_1u_{x1} + F_2u_{x2} + F_3u_{x3} + F_4u_{x4\dots} + F_9u_{x9} \\ u_y &= F_1u_{y1} + F_2u_{y2} + F_3u_{y3} + F_4u_{y4\dots} + F_9u_{y9} \\ u_z &= F_1u_{z1} + F_2u_{z2} + F_3u_{z3} + F_3u_{z3\dots} + F_9u_{z9} \end{aligned} \tag{4}$$

where $u_{x1}(y)$, ..., $u_{z9}(y)$ are the unknown variables of the problem and express the transitional displacement components of each of the nine points of the L9 element. The above displacement variables are the only unknowns, which their position are not on the beam element axis. Refined beam models can be obtained via using higher order Lagrange polynomials. Further, integration of LE on multi-domains can be used to refine some models.

On the other hand, the idea of the Taylor expansion model is based on Taylor polynomials that are used as generic functions in the displacement field over the cross section Filippi and Carrera

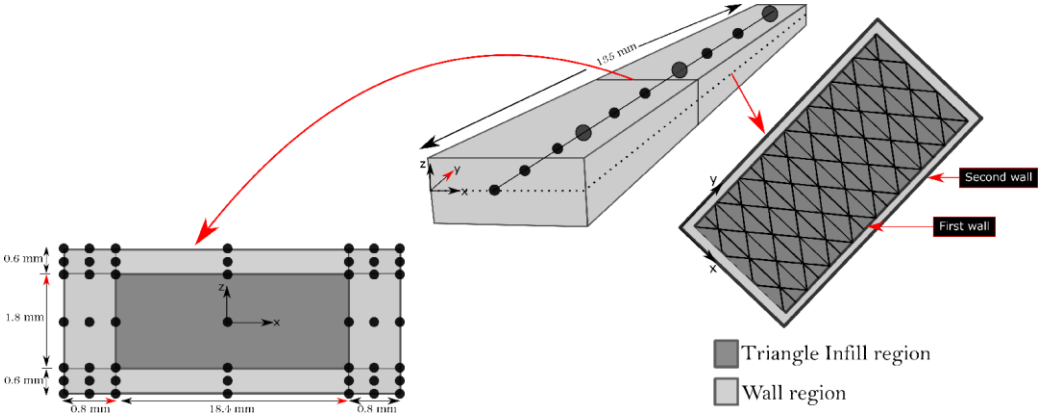

Fig. 2 Left: Cross section L9 expansion discretization, middle: FEM discretization four noded beam element, Right: Top view of the printing features of the infill region with triangular pattern

(2016). The order of expansion is presented as an input and can be arbitrary. For example, the second order, *N*=2 derives into the following displacement field

$$\begin{aligned} u_x &= u_{x_1} + xu_{x_2} + zu_{x_3} + x^2u_{x_4} + xzu_{x_5} + z^2u_{x_6} \\ u_y &= u_{y1} + xu_{y_2} + zu_{y_3} + x^2u_{y_4} + xzu_{y_5} + z^2u_{y_6} \\ u_z &= u_{z_1} + xu_{z_2} + zu_{z_3} + x^2u_{z_4} + xzu_{z_5} + z^2u_{z_6} \end{aligned} \tag{5}$$

Instead, each single LE element maintain its material and geometrical properties, then, assembled to compute the global stiffness matrix.

Both stiffness and mass matrices are computed by means of principle of virtual displacements as shown below

$$\delta L_{int} \int_V \delta \boldsymbol{\epsilon}^T \sigma dV = -\delta L_{ine} \tag{6}$$

where δL_{int} and δL_{ine} describe the virtual variation of strain energy and inertial loads, respectively. Hence, by using virtual nodal displacements, the internal strain energy and inertia contribution can be expressed as follows

$$\begin{aligned} \delta L_{int} &= \delta {q_{sj}}^T \boldsymbol{K}^{ij\tau s} q_{\tau i} \\ \delta L_{ine} &= \delta {q_{sj}}^T \boldsymbol{M}^{ij\tau s} \ddot{q}_{\tau i} \end{aligned} \tag{7}$$

in which, $\boldsymbol{K}^{ij\tau s}$ and $\boldsymbol{M}^{ij\tau s}$ refer to the fundamental nucleus of the stiffness and mass matrices, respectively. The superscripts used ($ij\tau s$) stand for the four indexes used to expand the element matrix, and the double dot stands for double derivative with respect to time. For more information and complete derivations reader can refer to Refs. (Carrera *et al*. 2014, Pagani and Sanchez-Majano 2021, Pagani *et al*. 2020, 2021).

2.1 High fidelity modeling of 3D printed structure

The advanced capabilities of CUF 1D beam models can be leveraged to model the multicomponent 3D printed structures. Multicomponent 3D printed structures represent most of the 3D printing structures produced via FDM. FDM structures are composed of different

components/regions, such as infill, wall, floor and roof. These components usually have various materials and geometrical behavior. In a MarkTwo printed structure, for instance, infill region can be of different material properties that cannot be added along with the same element of wall or floor/roof components. An efficient FE modelling of Multicomponent 3D printed structures often requires considering of each component separately with different elements to build sufficiently accurate models with a reasonable number of Degrees of Freedom (DOFs). A 3D printed beam is made of different layers, having each layer various components. In most cases, such beams can be modeled by adopting either the equivalent single layer (ESL) or layerwise (LW) approaches. ESL models a multilayered beam as an equivalent monolayer one. The LW retains each layer but with higher computational costs. The component wise (CW) exploits LE 1D elements to model each component of a structure separately and independently of their geometrical and material characteristics. LE formulation was presented to implement CW model to divide the FDM cross section into various sub domains, for instance, floor, infill as shown in Fig. 2.

Each component of the specimen is modelled using LE cross-sectional elements. In particular:

- LE formulation was presented to implement CW model to divide the FDM cross-section into various subdomains, see floor, walls and infill in Fig. 2 bottom left.
- Each component geometrical and material characteristics are retained.
- The CW approach does not need any coupling techniques, because the FE matrices of each element are formally the same as presented in Fig. 3.

CW models can be locally refined by using higher- or lower-order models where required. Such a feature leads to further computational cost reductions and multiscale modeling; 1D LE models can be concurrently applied to model layers (macroscale), matrix and fibres (microscale). This methodology can be very powerful when, for instance, voids at micro-scale or/and detailed

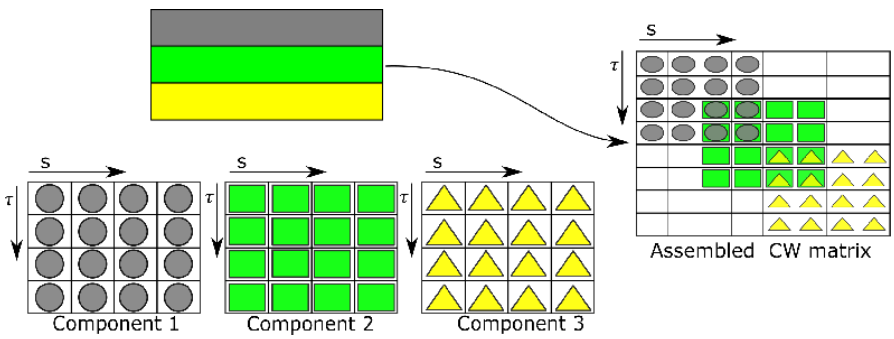

Fig. 3 Stiffness matrix assemblage schemes

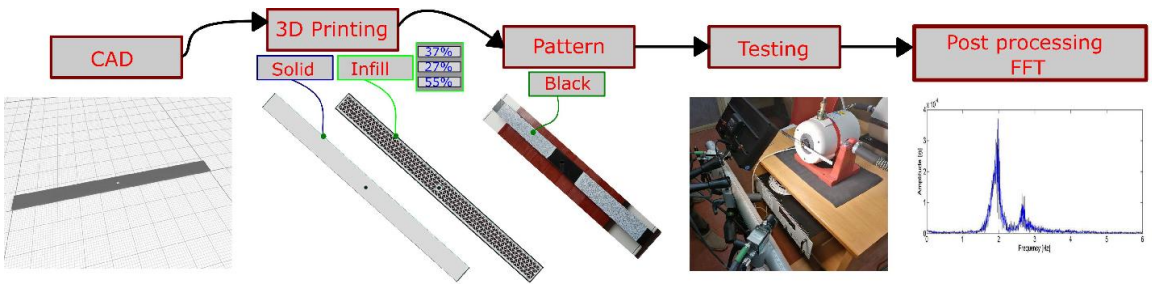

Fig. 4 Printing and experimental process Flowchart

stress fields are required in a specific portion of the structures. Fig. 3 shows the assembly strategies for a multicomponent structure stiffness matrix. In classical approaches, the structure is reduced to a single equivalent structure. In the CW, the stiffness matrix elements of different components are superimposed only at the interface level to impose the displacement continuity.

3. Experimental setup

Fig. 4 illustrates the flow chart of the experimental procedure steps. First, the geometry of the considered beams is designed by using a CAD software. Then we print the samples with different strategies; solid beams and then infill with different percentages as in Section 3.1. Before testing the specimens, white background with a black pattern has been used for the Digital Image Correlation (DIC) acquisition. Free vibration analysis was performed by an electro-dynamic shaker testing system as in Section 3.2. Lastly, the results have been acquired by means of a Q-400 DIC system via Fast Fourier transform (FFT).

3.1 Printing strategy

FDM is a layer wise 3D printing technology approach was used in this study. MarkTwo® (MT)-3D printer produced by Markforged® was used to print the specimens. MarkTwo printer is a compact printer with workspace of 320mm, 231mm, and 154mm in length, width and height, respectively, as shown in Fig. 5(a). Their features allow of producing thermoplastic, such as nylon and chopped carbon fiber embedded in nylon (Onyx) parts embedded with various types of continuous fiber reinforcements including carbon, glass, high strength high temperature (HSHT) fiberglass and Kevlar. MarkTwo consists of print bed, print head, two nozzles, each nozzle connected to material feeding system; the first feeding system is for printing matrix, whereas the other one for a reinforcement deposition as presented in Fig. 5(b). Both feeders are the same, however, a cutting tool is included in the reinforcement extruder to cut the fiber at specific length. The matrix material filament spool is fed to the extruder, which then pulls the filament from the spool into the tube towards the print head. Inside the printing head, Onyx is heated to 265°C, which is above the melting temperature, making the material ready to be deposited. MarkTwo

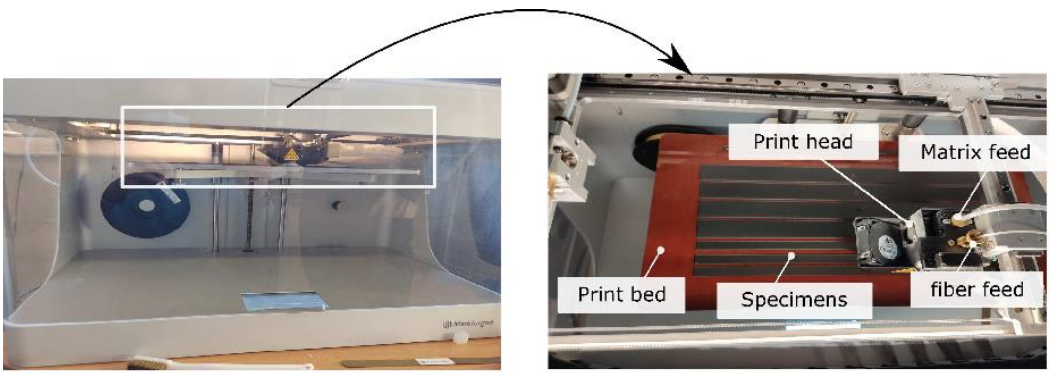

(a) MarkTwo printer (b) Top view printing procedure

Fig. 5 3D Printer apparatus

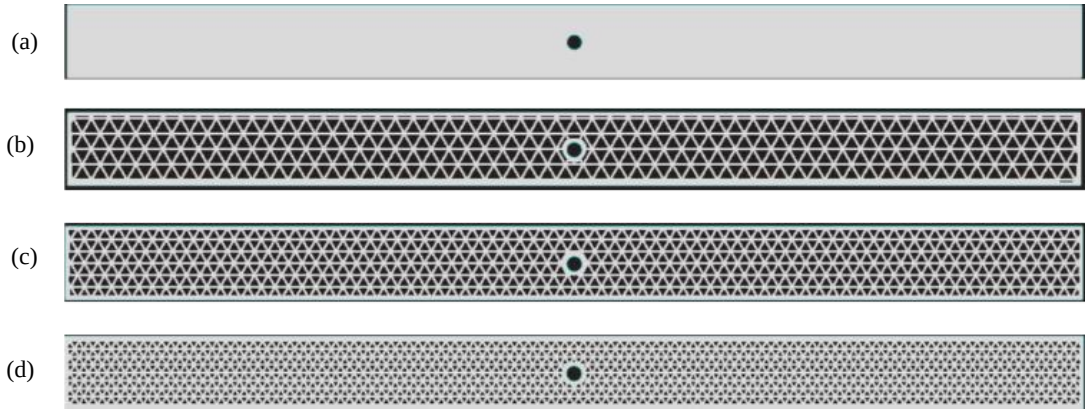

Fig. 6 (a) solid beam, (b) infill percentage of 28%, (c) infill percentage of 37%, (d) infill percentage of 55%

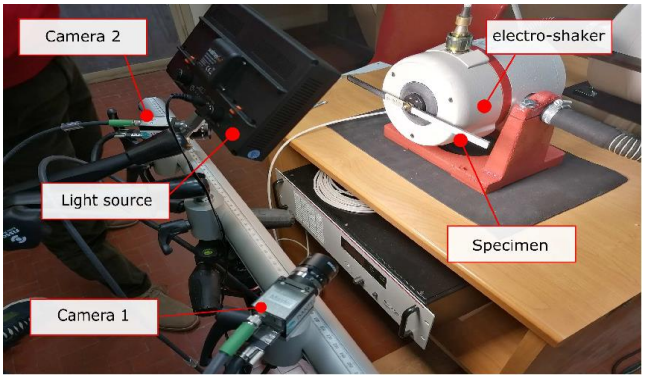

Fig. 7 Electro-dynamic shaker testing system with Digital Image Correlation

deposites only one type of material at a time that is either matrix filament or reinforcement. This work aims to characterize material properties in the solid beams and then for various infill material properties. Hence, firstly solid beam is considered including printing at least three layers of Onyx at the floor and roof regions, and two lateral polymeric material should be placed around the border of each layer. Then, the filling percentage can be arbitrary. Each layer has a thickness of 0.2 mm, as imposed by the slicing software. Fig. 6 shows the internal views of various infill FDM printed components.

3.1 Free vibration testing

An electro-dynamic shaker testing system by Brüel and Kjaer® was exploited to perform free vibration analysis as illustrated in Fig. 7. The testing system provides various range of frequencies.

The models have been excited by means of a random signal with a frequency content in the range between 1 Hz and 150 Hz, as shown by the signal spectra reported in Fig. 8(a). The random signal has been modulated with a sinusoidal function in order to smooth the excitation at the beginning of the test and at the end, see Fig. 8(b). The results have been acquired by means of a Q-400 DIC system by Dantec Dynamics®. Their features have the ability to capture true full field, non-contact and three dimensional shape, strains and various displacements on structure produced

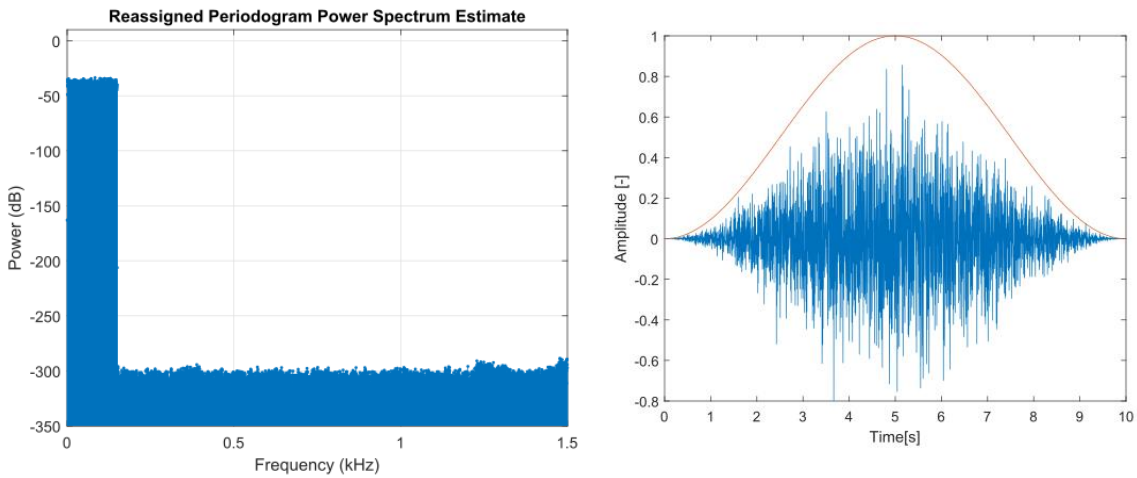

(a) Power spectrum of the random signal (b) Time history of the random signal

Fig. 8 Random signal used as input in the vibration test

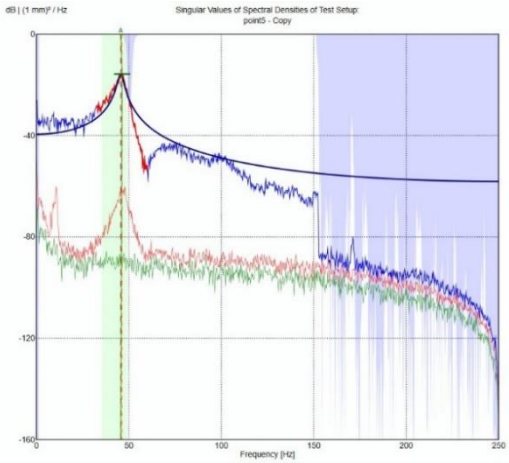

Fig. 9 Singular values of spectral densities of test setup

with almost any material. The DIC equipment, shown in Fig. 7, is composed of 2 megapixel cameras for high-frequency image tracking, one light source and data acquisition unit. Further, image processing is carried out with the licensed software tool Instra4D V2.1. FFTs are mainly used to visualize frequencies by capturing the maximum value as shown in Fig. 9.

4. Numerical analysis and results

To validate the capabilities of proposed CUF-based CW modeling approach, several FDM laminated beams comprising different geometrical features and infill percentages are compared with experimental results. Table 1 reports the models that have been considered. In Table 1, W_N and T_N indicate the nominal width and thickness, respectively of the beams considered. Instead,

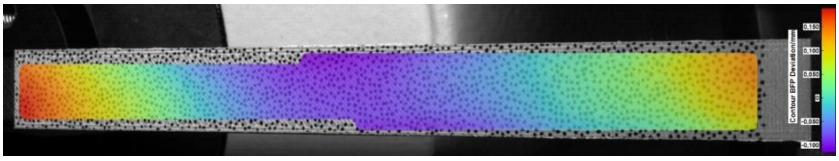

Fig. 10 Example of DIC displacement full field

Table 1 Printed specimens infill percentages and dimensions obtained by slicing software and experimentally

Name	Infill [%]	W_N [mm]	T_N [mm]	W_{exp} [mm]	T_{exp} [mm]
100SW10T3	100	10	3	9.990	3.064
100SW10T4.5	100	10	4.5	9.964	4.472
100SW10T6	100	10	6	9.985	6.026
100SW10T3	100	20	3	20.034	2.948
28TRI20T3	28	20	3	20.008	3.060
37TRI20T3	37	20	3	20.005	3.064
55TRI20T3	55	20	3	19.960	2.906

W_{exp} and T_{exp} are the width and thickness measured experimentally, respectively. It is shown that parts were printed with high accuracy for width with 0.1% error and less accuracy for thickness with 1.5% error. The dynamic test has been carried out by performing a free vibration analysis using a random excitation. Fig. 11 shows the specimens before the testing, in which white background with a black pattern has been used for the DIC acquisition. For the sake of completeness, a convergence study for different discretization on the cross section, from lower order to higher order was carried out. Since the scope of this work is to predict the modulus of elasticity of various infill percentages, we firstly considered solid beam with various geometries (mainly different thicknesses) to predict the elastic modulus of the Onyx. Then we considered different beams with different infill percentages to characterize infill material properties.

4.1 Convergence study

The beam used for the convergence study has the following geometrical features: length of 135 mm, 4.5 mm height, and 10 mm width as presented in Fig. 12(a). The material used is Onyx for the whole beam and their material properties was adopted from Markforged datasheet of 3.6 GPa and 1200 kg/m^3 of modulus of elasticity and material density, respectively. The material used for the whole beam is isotropic and its constitutive relations is based on a linear behavior and all of those convergence study models have the same boundary condition. The results from the convergence study solutions are compared with those from 3D solid models by using the commercial software ABAQUS analysis user's manual (2016). Table 2 shows the comparison of first 5 natural frequencies with different element types used, including the comparison between LE and TE models. For the sake of brevity, only one ABAQUS model is introduced for comparison. The convergence study results reveal that 8-B4+Q9 is sufficient to have a converged model and show strong agreement with the ABAQUS result.

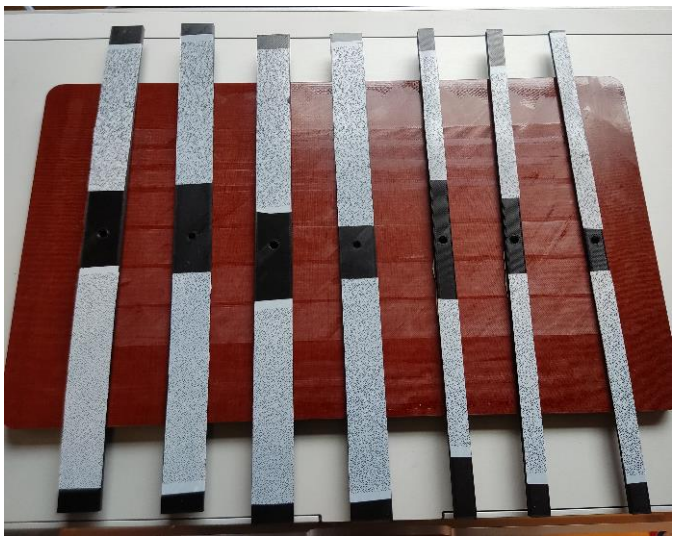

Fig. 11 Specimens before the test

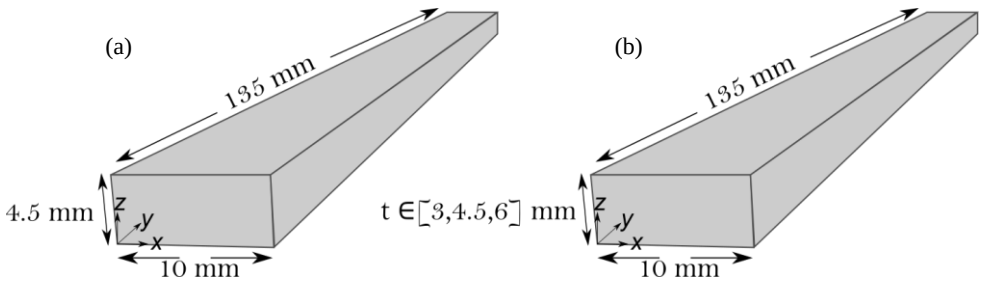

Fig. 12 (a) FDM printed solid beam used for convergence study, (b) infill beams considered for material characterization

Table 2 Convergence study results, first 5 natural frequency [hz]

Mesh	DOF	f_1	f_2	f_3	f_4	f_5
Solid(C3D20R)	4029	69.67	153.53	434.55	937.61	1207.80
LE models						
2-B4+Q9	189	72.83	160.43	453.79	983.27	1508.28
4-B4+Q9	351	70.79	156.26	442.20	956.93	1234.51
6-B4+Q9	513	70.21	155.10	438.09	949.13	1218.44
8-B4+Q9	675	69.96	154.56	436.41	946.13	1213.44
10-B4+Q9	837	69.82	154.26	435.53	944.32	1210.80
TE models						
8-B4-TE1	225	69.02	152.91	252.40	430.52	936.31
8-B4-TE2	450	69.96	154.58	436.41	946.25	1213.45

4.2 Solid beam material characterization

The solid beams have the following geometrical features: length of 135 mm, 10 mm width, and

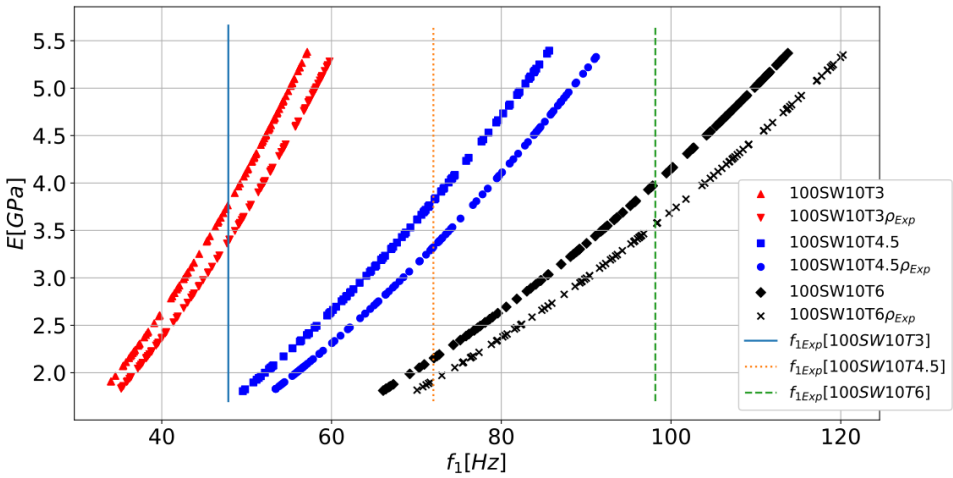

Fig. 13 Scatter plots comparing the frequency for first mode of the various FDM solid beams

Table 3 Validation of results between experimental ad CUF-CW modeling of solid beams

Model	f_1 Exp-[hz]	f_1 CUF-[hz]	E_d- [GPa]	E_I-[GPa]
100SW10T3	47.846	47.843	3.600	3.384
100SW10T4.5	72.003	71.993	3.600	3.323
100SW10T6	98.156	98.152	3.600	3.563

three different heights of 3, 4.5, and 6 mm as shown in Fig. 12(b) and their internal view shown in Fig. 6(a). Two scenarios of 100 random simulations were performed. Firstly, a set of 100 randomly generated values of the Onyx Young's modulus, ranging from $E_{O_r} \in [0.5E_O, \dots, 1.5E_O]$ GPa. The density captured from Markforged data-sheet of 1200 kg/m^3 was kept. E_{O_r} and E_O refer to randomly generated values of elastic modulus of Onyx and modulus of elasticity of Onyx from the MT data sheet, respectively. The second scenario, is same as the previous one but with the densities values obtained experimentally that are of 1076, 1046, and 1070 kg/m^3 for 100SW20T3, 100SW20T4.5, and 100SW20T6, respectively. Both scenarios are compared for different geometrical features. Based on the convergence study results, simulations are modeled by means of 8 B4 finite elements along the *y*-axis and a quadratic approximation of L9 was used. The first frequency provided by the FEM simulations are stored to create a database. Fig. 13 illustrates a comparison between the two scenarios results of first natural frequency mode based on possible input parameters of Young's modulus with density adopted from data sheet and experimental results. The inverse characterization then allows finding the elastic modulus of the input parameters starting by reading the information on the required set of the output achieved experimentally as shown by the vertical lines in Fig. 13. Table 3 reports a comparison between the predicted results of the first natural frequency mode and the results obtained experimentally by DIC. In which the obtained modulus of elasticity based on the inverse characterization are reported for each case in Table 3. f_1-Exp represents the obtained experimental results and $CUF_{\rho e}$ refers to the numerical results calculated with the densities obtained experimentally and mentioned earlier. E_d and E_I are the modulus of elasticity provided by the data sheet and by inverse method, respectively.

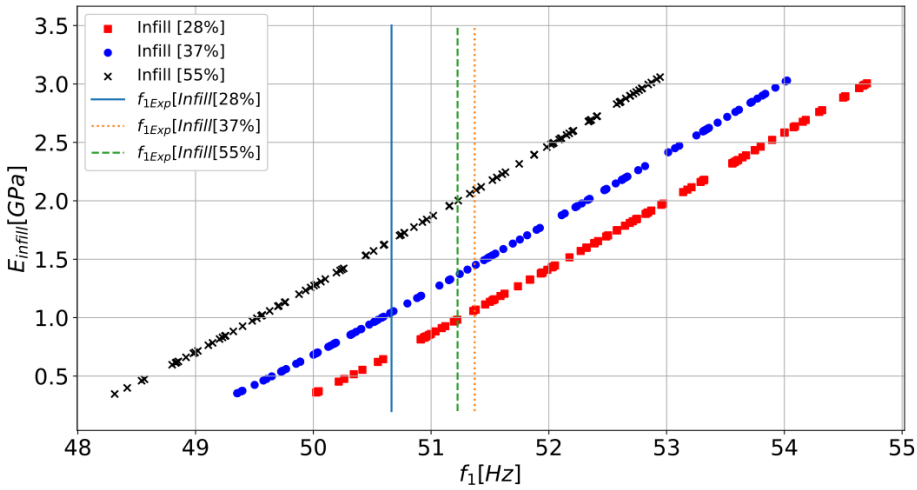

Fig. 14 Scatter plots comparing the observed frequency for first mode of the various FDM infill beams

Table 4 Validation of results between experimental ad CUF-CW modeling of various Infill percentages

Model	f_1 Exp-[hz]	f_1 CUF-[hz]	E_I- [GPa]	ρ_e-[Kg/m^3]
100SW20T3	46.077	48.568	-	3.384
28TRI20T3	50.664	50.664	0.682	622.000
37TRI20T3	51.370	51.972	1.446	662.000
55TRI20T3	51.225	51.028	1.997	728.000

The results revealed that, material properties predicted are very close for the various geometrical features considered, and a bit lower compared to data sheet provided by Markforged® as expected.

4.3 Influence of infill

The infill beam considered has the following geometrical features: length of 135 mm, 3 mm height, and 20 mm of width to allow for more infill effect and their internal views in Fig. 6(b)-(d). The infilled beams considered have three layers in floor and roof regions, each layer of 0.2 mm, whereas the infill region has 9 layers, each layer of 0.2 mm. A set of 100 randomly generated values where Young's modulus of Onyx varies in the range between 0.1 and 0.9 E ($E_{O_r} \in [0.5E_O, \dots, 1.5E_O]$). The densities of the infilled parts used in the numerical results were measured experimentally. For instance, 622, 662 and 728 kg/m^3 correspond to the 28%, 37% and 55% infill, respectively. The dynamic response outputs from the simulations were stored to create a database. Fig. 14 presents the results of first natural frequency mode based on possible input parameters of Young's modulus with density adopted experimentally for various infill percentages. Table 4 gathers the predicted results of the numerical first natural frequency mode and the results obtained experimentally by the means of DIC for various beams with different infill percentages. In addition, Table 4 reports the predicted modulus of elasticity of infill region based on the inverse characterization for the 28%, 37%, and 55% infill percentages. f_1-Exp is the experimental fundamental frequency and *f*1-*CUF* refers to the numerical results obtained via CUF-CW model.

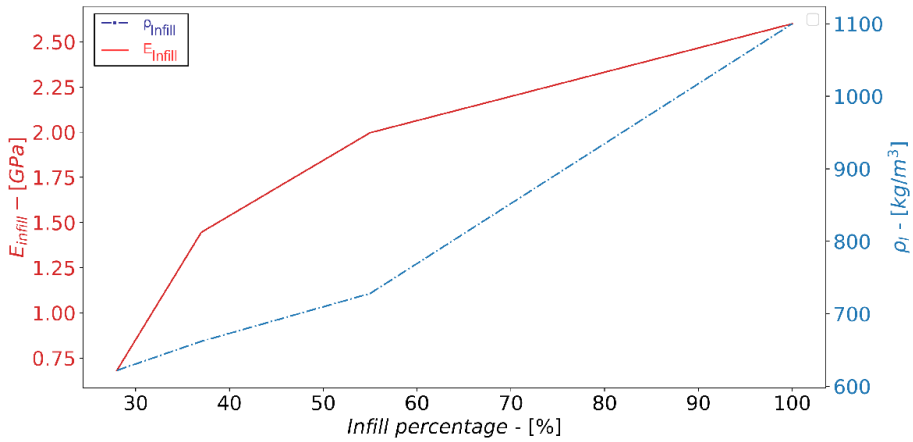

Fig. 15 Results of E_I with different infill percentages

E_I is the modulus of elasticity obtained by inverse method through the experimental results as shown by the vertical lines in Fig. 14, and ρ_e is the density of the considered infill beams obtained experimentally.

The results show that, the infill material properties are increased by increasing the percentage of the infill as expected. Also infill region material properties shown a huge sensitivity based on the density of the infill part. Therefore, it is important to consider the correct value of the infill material properties to get an accurate simulation outcome, which can be used later in advanced mechanical studies such as optimization of 3D printed parts. Fig. 15 reports the infill Young's modulus based on various infill percentages and density of the infill part. ρ_I refers to the density of the infill component obtained experimentally. The results revealed that by increasing the infill percentage, the infilled modulus of elasticity and density raised as expected.

5. Conclusions

The aim of this work was to explore the capability of using CUF-CW modeling approach to model the free vibration analysis of FDM printed structures, and the retrieval of the mechanical properties for different geometrical features and infill percentages. Lagrange and Taylor polynomials, are applied to discretize the beam cross-sectional kinematics. The proposed numerical model have been used to develop a driven database via free vibration analysis, which were then used to predict the elastic modulus of different regions within the printed structure based on inverse characterization. The obtained numerical results have been compared to experimental work to verify the modeling accuracy. The advantages and novelties of the proposed tool can be concluded as the following:

- The results show that the current proposed numerical tool CUF-CW approach can properly estimate the natural frequencies, and modes of the sandwich beams. The main advantages of this tool is that it can deal with higher order effects, without any assumptions and very low computational cost compared to 3D solid FE.
- CUF-CW model analyses were found to be computationally efficient to simulate the FDM printed coupons using a 1D FE.

- Infill material properties are very sensitive to the infill density, which affects on the accuracy of the simulation. This might be of utmost importance in optimization problems.

On-going work is focused on including more parameters such as number of walls, different materials including fibers, fibre orientations, etc. The influence of those features could be used for the optimization of a desired mechanical response of 3D printed components.

Acknowledgment

Mohamed Refat acknowledges the support from the Italian Ministry of Foreign Affairs and International Cooperation (MAECI) under PhD fellowships scheme for foreign and Italian citizens living abroad awarded by the Italian Government.

References

ABAQUS Analysis User's Manual (2016), Dassault Systemes Simulia Corp.

Afrose, M.F., Masood, S.H., Iovenitti, P., Nikzad, M. and Sbarski, I. (2019), "Effects of part build orientations on fatigue behaviour of FDM-processed PLA material", *Progr. Addit. Manuf.*, **1**(1), 21-28. https://doi.org/10.1007/s40964-015-0002-3.

Akhoundi, B. and Behravesh, A.H. (2019), "Effect of filling pattern on the tensile and flexural mechanical properties of fdm 3d printed products", *Exp. Mech.*, **59**(6), 883-897. https://doi.org/10.1007/s11340-018-00467-y.

Al Abadi, H., Thai, H.T., Paton-Cole, V. and Patel, V.I. (2018), "Elastic properties of 3D printed fibre-reinforced structures", *Compos. Struct.*, **193**, 8-18. https://doi.org/10.1016/j.compstruct.2018.03.051.

Azzara, R., Carrera, E., Filippi, M. and Pagani, A. (2020), "Time response stress analysis of solid and reinforced thin-walled structures by component-wise models", *Int. J. Struct. Stab. Dyn.*, **20**(14), 2043010. https://doi.org/10.1142/S0219455420430105.

Bárnik, F., Vaško, M., Handrik, M., Dorčiak, F. and Majko, J. (2019), "Comparing mechanical properties of composites structures on onyx base with different density and shape of fill", *Transp. Res. Procedia*, **40**, 616-622. https://doi.org/10.1016/j.trpro.2019.07.088.

Berretta, S., Davies, R., Shyng, Y.T., Wang, Y. and Ghita, O. (2017), "Fused deposition modelling of high temperature polymers: Exploring CNT peek composites", *Polym. Test.*, **63**, 251-262. https://doi.org/10.1016/j.polymertesting.2017.08.024.

Caminero, M.A., Chacón, J.M., García-Moreno, I. and Reverte, J.M. (2018), "Interlaminar bonding performance of 3d printed continuous fibre reinforced thermoplastic composites using fused deposition modelling", *Polym. Test.*, **68**, 415-423. https://doi.org/10.1016/j.polymertesting.2018.04.038.

Carrera, E. and Petrolo, M. (2012), "Refined beam elements with only displacement variables and plate/shell capabilities", *Meccanica*, **47**(3), 537-556. https://doi.org/10.1007/s11012-011-9466-5.

Carrera, E., Cinefra, M., Petrolo, M. and Zappino, E. (2014), *Finite Element Analysis of Structures through Unified Formulation*, John Wiley & Sons.

Carrera, E., de Miguel, A.G. and Pagani, A. (2017), "Hierarchical theories of structures based on legendre polynomial expansions with finite element applications", *Int. J. Mech. Sci.*, **120**, 286-300. https://doi.org/10.1016/j.ijmecsci.2016.10.009.

Carrera, E., Giunta, G. and Petrolo, M. (2011), *Beam Structures: Classical and Advanced Theories*, John Wiley & Sons.

Chacón, J.M., Caminero, M.A., García-Plaza, E. and Núnez, P.J. (2017), "Additive manufacturing of pla structures using fused deposition modelling: Effect of process parameters on mechanical properties and their optimal selection", *Mater. Des.*, **124**, 143-157. https://doi.org/10.1016/j.matdes.2017.03.065.

Chu, T.C., Ranson, W.F. and Sutton, M.A. (1985), "Applications of digital-image-correlation techniques to experimental mechanics", *Exp. Mech.*, **25**(3), 232-244.

Coelho, A.M.G., Mottram, J.T. and Harries, K.A. (2015), "Finite element guidelines for simulation of fibre-tension dominated failures in composite materials validated by case studies", *Compos. Struct.*, **126**, 299-313. https://doi.org/10.1016/j.compstruct.2015.02.071.

Cuellar, J.S., Smit, G., Plettenburg, D. and Zadpoor, A. (2018), "Additive manufacturing of non-assembly mechanisms", *Addit. Manuf.*, **21**, 150-158. https://doi.org/10.1016/j.addma.2018.02.004.

Dai, Y., Wang, H., Wu, G., Wan, J., Cao, S., Yang, F. and He, X. (2017), "Behavior investigation of cfrp-steel composite members using digital image correlation", *Int. Digital Imag. Correl. Soc.*, 129-132.

Ding, S., Zou, B., Wang, P. and Ding, H. (2019), "Effects of nozzle temperature and building orientation on mechanical properties and microstructure of peek and PEI printed by 3D-FDM", *Polym. Test.*, **78**, 105948. https://doi.org/10.1016/j.polymertesting.2019.105948.

Durgun, İ. and Ertan, R. (2014), "Experimental investigation of fdm process for improvement of mechanical properties and production cost", *Rapid Prototyp. J.*, **20**(3), 228-235. https://doi.org/10.1108/RPJ-10-2012-0091.

Ferreira, R.T.L., Amatte, I.C., Dutra, T.A. and Bürger, D. (2017), "Experimental characterization and micrography of 3d printed pla and pla reinforced with short carbon fibers", *Compos. Part B: Eng.*, **124**, 88-100. https://doi.org/10.1016/j.compositesb.2017.05.013.

Filippi, M. and Carrera, E. (2016), "Capabilities of 1D CUF-based models to analyse metallic/composite rotors", *Adv. Aircraft Spacecraft Sci.*, **3**(1), 1. https://doi.org/10.12989/aas.2016.3.1.001.

Gao, W., Zhang, Y., Ramanujan, D., Ramani, K., Chen, Y., Williams, C.B., ... & Zavattieri, P.D. (2015), "The status, challenges, and future of additive manufacturing in engineering", *Comput. Aid. Des.*, **69**, 65-89. https://doi.org/10.1016/j.cad.2015.04.001.

Gibson, I., Rosen, D.W., Stucker, B., Khorasani, M., Rosen, D., Stucker, B. and Khorasani, M. (2021), *Additive Manufacturing Technologies*, **17**, Cham, Switzerland.

Goh, G.D., Sing, S.L. and Yeong, W.Y. (2021), "A review on machine learning in 3d printing: applications, potential, and challenges", *Artif. Intel. Rev.*, **54**(1), 63-94. https://doi.org/10.1007/s10462-020-09876-9.

Gordelier, T.J., Thies, P.R., Turner, L. and Johanning, L. (2019), "Optimising the fdm additive manufacturing process to achieve maximum tensile strength: A state-of-the-art review", *Rapid Prototyp. J.*, **25**(6), 953-971. https://doi.org/10.1108/RPJ-07-2018-0183.

Hofstätter, T., Pedersen, D.B., Tosello, G. and Hansen, H.N. (2017), "State-of-the-art of fiber-reinforced polymers in additive manufacturing technologies", *J. Reinf. Plast. Compos.*, **36**(15), 1061-1073. https://doi.org/10.1177/0731684417695648.

Ivey, M., Melenka, G.W., Carey, J.P. and Ayranci, C. (2017), "Characterizing short-fiber-reinforced composites produced using additive manufacturing", *Adv. Manuf.: Polym. Compos. Sci.*, **3**(3), 81-91. https://doi.org/10.1080/20550340.2017.1341125.

Kumar, L.J. and Krishnadas Nair, C.G. (2017), "Current trends of additive manufacturing in the aerospace industry", *Advances in 3D Printing & Additive Manufacturing Technologies*, 39-54. https://doi.org/10.1007/978-981-10-0812-2_4.

Lay, M., Thajudin, N.L.N., Hamid, Z.A.A., Rusli, A., Abdullah, M.K. and Shuib, R.K. (2019), "Comparison of physical and mechanical properties of PLA, abs and nylon 6 fabricated using fused deposition modeling and injection molding", *Compos. Part B*, **176**, 107341. https://doi.org/10.1016/j.compositesb.2019.107341.

Lee, J.Y., An, J. and Chua, C.K. (2017), "Fundamentals and applications of 3D printing for novel materials", *Appl. Mater. Today*, **7**, 120-133. https://doi.org/10.1016/j.apmt.2017.02.004.

Li, L., Sun, Q., Bellehumeur, C. and Gu, P. (2002), "Composite modeling and analysis for fabrication of FDM prototypes with locally controlled properties", *J. Manuf. Proc.*, **4**(2), 129-141. https://doi.org/10.1016/S1526-6125(02)70139-4.

Ma, C., Faust, J. and Roy-Mayhew, J.D. (2021), "Drivers of mechanical performance variance in 3d-printed fused filament fabrication parts: An onyx FR case study", *Polym. Compos.*, **42**(9), 4786-4794. https://doi.org/10.1002/pc.26187.

Markforged (2015), Markforged Composite 3D Printers. Available from: https://markforged.com/products/.

Masrol, S.R. and Siswanto, W.A. (2014), "Stress concentration analysis of plate with circular hole: Elasticity theory and finite element comparison", *Appl. Mech. Mater.*, **465**, 1385-1389. https://doi.org/10.4028/www.scientific.net/AMM.465-466.1385.

Melenka, G.W., Cheung, B.K., Schofield, J.S., Dawson, M.R. and Carey, J.P. (2016), "Evaluation and prediction of the tensile properties of continuous fiber-reinforced 3d printed structures", *Compos. Struct.*, **153**, 866-875. https://doi.org/10.1016/j.compstruct.2016.07.018.

Miri, V., Persyn, O., Lefebvre, J.M. and Seguela, R. (2009), "Effect of water absorption on the plastic deformation behavior of nylon 6", *Eur. Polym. J.*, **45**(3), 757-762. https://doi.org/10.1016/j.eurpolymj.2008.12.008.

Ning, F., Cong, W., Qiu, J., Wei, J. and Wang, S. (2015), "Additive manufacturing of carbon fiber reinforced thermoplastic composites using fused deposition modeling", *Compos. Part B: Eng.*, **80**, 369-378. https://doi.org/10.1016/j.compositesb.2015.06.013.

Pagani, A. and Sanchez-Majano, A.R. (2021), "Stochastic stress analysis and failure onset of variable angle tow laminates affected by spatial fibre variations", *Compos. Part C: Open Access*, **4**, 100091. https://doi.org/10.1016/j.jcomc.2020.100091.

Pagani, A., Azzara, R., Augello, R., Carrera, E. and Wu, B. (2020), "Accurate through-the-thickness stress distributions in thin-walled metallic structures subjected to large displacements and large rotations", *Vietnam J. Mech.*, **42**(3), 239-254. https://doi.org/10.15625/0866-7136/15042.

Pagani, A., Enea, M. and Carrera, E. (2021), "Component-wise damage detection by neural networks and refined FEs training", *J. Sound Vib.*, **509**, 116255. https://doi.org/10.1016/j.jsv.2021.116255.

Pagani, A., Enea, M. and Carrera, E. (2022), "Quasi-static fracture analysis by coupled three-dimensional peridynamics and high order one-dimensional finite elements based on local elasticity", *Int. J. Numer. Meth. Eng.*, **123**(4), 1098-1113. https://doi.org/10.1002/nme.6890.

Pagani, A., Petrolo, M. and Carrera, E. (2014), "Flutter analysis by refined 1d dynamic stiffness elements and doublet lattice method", *Adv. Aircraft Spacecraft Sci.*, **1**(3), 291. https://doi.org/10.12989/aas.2014.1.3.291.

Parandoush, P. and Lin, D. (2017), "A review on additive manufacturing of polymer-fiber composites", *Compos. Struct.*, **182**, 36-53. https://doi.org/10.1016/j.compstruct.2017.08.088.

Penumakala, P.K., Santo, J. and Thomas, A. (2020), "A critical review on the fused deposition modeling of thermoplastic polymer composites", *Compos. Part B: Eng.*, **201**, 108336. https://doi.org/10.1016/j.compositesb.2020.108336.

Petrolo, M., Carrera, E. and Alawami, A.S.A.S. (2016), "Free vibration analysis of damaged beams via refined models", *Adv. Aircraft Spacecraft Sci.*, **3**(1), 95. https://doi.org/10.12989/aas.2016.3.1.095.

Rajpurohit, S.R. and Dave, H.K. (2018), "Effect of process parameters on tensile strength of FDM printed PLA part", *Rapid Prototyp. J.*, **24**(8), 1317-1324. https://doi.org/10.1108/RPJ-06-2017-0134.

Refat, M., Luzi, L., Agostini, L., Pucci, R., Berselli, G. and Vertechy, R. (2021), "Fused filament fabrication of continuous fiber-reinforced thermoplastics for compliant mechanisms", *Smart Mater., Adapt. Struct. Intel. Syst.*, **85499**, V001T07A015. https://doi.org/10.1115/SMASIS2021-68331.

Sanei, S.H.R. and Popescu, D. (2020), "3D-printed carbon fiber reinforced polymer composites: a systematic review", *J. Compos. Sci.*, **4**(3), 98. https://doi.org/10.3390/jcs4030098.

Shen, J., Pagani, A., Arruda, M.R.T. and Carrera, E. (2022), "Exact component-wise solutions for 3d free vibration and stress analysis of hybrid steel-concrete composite beams", *Thin Wall. Struct.*, **174**, 109094. https://doi.org/10.1016/j.tws.2022.109094.

Tekinalp, H.L., Kunc, V., Velez-Garcia, G.M., Duty, C.E., Love, L.J., Naskar, A.K., ... & Ozcan, S. (2014), "Highly oriented carbon fiber-polymer composites via additive manufacturing", *Compos. Sci. Technol.*, **105**, 144-150. https://doi.org/10.1016/j.compscitech.2014.10.009.

Turner, B.N. and Gold, S.A. (2015), "A review of melt extrusion additive manufacturing processes: Ii. materials, dimensional accuracy, and surface roughness", *Rapid Prototyp. J.*, **21**(3), 250-261. https://doi.org/10.1108/RPJ-02-2013-0017.

Turner, B.N., Strong, R. and Gold, S.A. (2014), "A review of melt extrusion additive manufacturing

processes: I. Process design and modeling", *Rapid Prototyp. J.*, **20**(3), 192-204. https://doi.org/10.1108/RPJ-01-2013-0012.

Vălean, C., Marșavina, L., Mărghitaș, M., Linul, E., Razavi, J. and Berto, F. (2020), "Effect of manufacturing parameters on tensile properties of FDM printed specimens", *Procedia Struct. Integr.*, **26**, 313-320. https://doi.org/10.1016/j.prostr.2020.06.040.

Valentin, D., Paray, F. and Guetta, B. (1987), "The hygrothermal behaviour of glass fibre reinforced Pa66 composites: A study of the effect of water absorption on their mechanical properties", *J. Mater. Sci.*, **22**(1), 46-56. https://doi.org/10.1007/BF01160550.

Van Der Klift, F., Koga, Y., Todoroki, A., Ueda, M., Hirano, Y. and Matsuzaki, R. (2016), "3D printing of continuous carbon fibre reinforced thermo-plastic (CFRTP) tensile test specimens", *Open J. Compos. Mater.*, **6**(01), 18. https://doi.org/10.4236/ojcm.2016.61003.

Van Der Klift, F., Koga, Y., Todoroki, A., Ueda, M., Hirano, Y. and Matsuzaki, R. (2017), "3d printing of polymer matrix composites: A review and prospective", *Compos. Part B: Eng.*, **110**, 442-458. https://doi.org/10.1016/j.compositesb.2016.11.034.

Zadpoor, A.A. and Malda, J. (2017), "Additive manufacturing of biomaterials, tissues, and organs", *Ann. Biomed. Eng.*, **45**(1), 1-11. https://doi.org/10.1007/s10439-016-1719-y.

Zappino, E., Filippi, M., Pagani, A., Petiti, M. and Carrera, E. (2020), "Experimental and numerical analysis of 3D printed open-hole plates reinforced with carbon fibers", *Compos. Part C: Open Access*, **2**, 100007. https://doi.org/10.1016/j.jcomc.2020.100007.

EC